European Journal of Applied Sciences – Vol. 13, No. 02
Publication Date: April 25, 2025
DOI:10.14738/aivp.1302.18576.
Dath, H., Kannan, S., & Radhika, V. N. (2025). Coherent Manipulation of Ultra Cold Atoms Towards Mobile Gravimetry. European Journal of Applied Sciences, Vol - 13(02). 390-399.

Coherent Manipulation of Ultra Cold Atoms Towards Mobile Gravimetry

Hriday Dath
ISRO Inertial Systems Unit,
Thiruvananthapuram, 695013, India

Kannan, S.
ISRO Inertial Systems Unit,
Thiruvananthapuram, 695013, India

Radhika, V. N.
ISRO Inertial Systems Unit,
Thiruvananthapuram, 695013, India

ABSTRACT

Atom interferometry as a rapidly growing field has garnered a lot of interest in recent years for developing extremely accurate quantum sensors. It has been demonstrated by numerous research groups worldwide for a wide range of applications. In this work, we demonstrate the coherent manipulation of ultra-cold Rubidium (^{87}Rb) atoms with Raman laser pulses in the transportable gravimeter setup based on cold atom interferometry developed at ISRO Inertial Systems Unit. The achievement of coherent manipulation is carried out by demonstrating the Rabi oscillations in ultra-cold ensemble. The obtained oscillation frequency is found to be very well matching with the theoretical calculation. Subsequently, we demonstrate Ramsey fringes by applying two $\pi/2$ pulses with a time gap depending on Rabi oscillation frequency.

Keywords: Laser cooling, Two-photon transition, Rabi oscillation, Ramsey fringes.

INTRODUCTION

Cold atoms based sensors are pursued as the main tool for ultra-sensitive measurements in myriad of applications like inertial sensing, gravity mapping and fundamental research [1]–[3], [7]–[9]. Extensive research has been going on to use the cold atom sensors for real-world applications [10]–[15], mainly due to their unprecedented accuracy and long term stability. One of the initial steps towards developing such a sensor is to coherently manipulate the cold atoms with lasers. A recent work was carried out on the coherent manipulation of trapped atoms with frequency chirped laser pulses [16]. For that, it is desirable to generate cold sample of atoms with the population residing in one of the quantum states [17]–[19].

Portable atom interferometry based gravity sensors have been in development for many years, in many universities [25], [26] and some commercial products are available in market [12], [28]. Substantial efforts are being made towards development of the sensors with reduced size, weight, and power requirements while being robust enough for use in field applications [29],

[30]. In the present work, we discuss the experimental configuration for atom cloud generation and Raman beam interaction in the laboratory setup designed for transportable gravimeters.

Using coils for magnetic field compensation, we have achieved sub-Doppler cooling of ^{87}Rb to a temperature of $\sim 9\mu K$ [27] by employing Polarization Gradient Cooling. The atoms are then released from the trap and are subjected to two photon transition by interacting with laser beams, to obtain the coherent population transfer. Complete characterization of the atom laser interaction is necessary to ascertain the Rabi oscillation frequency as well as the duration of $\pi/2$, π pulses. This step holds paramount importance in realizing atom interferometry as it determines the key parameters that dictate the accuracy of cold atom gravimeter. In the present work, we have generated and studied the coherent superpositions of hyperfine levels of ^{87}Rb trapped and cooled in a transportable Ti-UHV chamber designed for gravimetric studies.

We have arranged the present work as follows: First, we briefly discuss the theory of coherent manipulation of atoms using stimulated Raman transitions, along with our experimental investigation. In sec. III, we describe the experimental setup. The theory of Ramsey fringes and the experimental results are elaborated in sec. III, and in sec. IV, we conclude the paper.

COHERENT MANIPULATION OF ATOMS

A Raman transition is the stimulated transfer of atom populations between two internal states via a virtual state. The beams used to drive the transitions are called Raman beams, and they are energetically separated by the energy difference between the energies of the two level. The virtual state is detuned (Δ) from an excited state in order to suppress spontaneous emission. This two-photon process is a standard way of achieving superposition states [20], [21]. These beams of specific duration are used to create atomic mirrors and beam splitters which creates the atomic wave function in desired superposition states for atom interferometry.

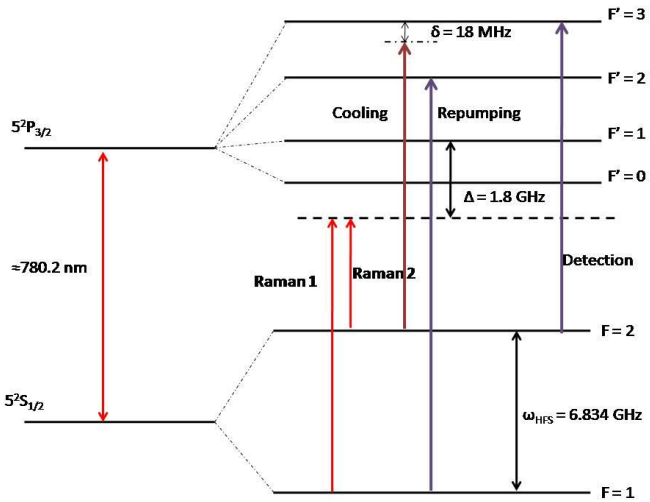

Figure 1: Energy level diagram of ^{87}Rb for the D2 line and the levels chosen for Raman transition. The plot is not drawn to scale.

Coherent manipulation of matter waves through two photon Raman transition can be performed by characterizing Rabi oscillations. In our experiment, we consider the D2 line

(~780.2 nm) of 87Rb. The atoms are prepared in ground state F = 1 after cooling and are released from the trap. Subsequently they are interacted with Raman beams passing vertically through the chamber.

The Hamiltonian excluding the spontaneous emission for our system is written as

$$H = \frac{p^2}{2m} + \hbar\omega_e|e\rangle\langle e| + \hbar\omega_g|g\rangle\langle g| + \hbar\omega_i|i\rangle\langle i| - d.E, \quad (1)$$

where m is the mass of Rb atom. $|g\rangle, |e\rangle$ are the two ground levels of the system, and $|i\rangle$ is the intermediate level. The last term is the light-atom interaction Hamiltonian. The driving electric field E consists of two frequency components and is given by.

$$E = E_1 \cos(k_1.r - \omega_1 t) + E_2 \cos(k_2.r - \omega_2 t). \quad (2)$$

Here ω_1 and ω_2 are the two laser beam frequencies with wave vectors k_1 and k_2 respectively.

As shown in the energy level diagram in Fig. 1, the two Raman beams frequencies are near resonant with allowed optical transition but far detuned. In these conditions, the three level system can be reduced to a two photon Raman transition as described by Kasevich and Chu [22]. The effective Rabi frequency Ω_{eff}, between the two ground states $|g\rangle, |e\rangle$ becomes

$$|\Omega_{eff}| = \frac{\Omega_e{}^*\Omega_g}{2\Delta}, \quad (3)$$

Where

$$\Omega_{g,e} = -\frac{\langle i|d.E_{1,2}|g,e\rangle}{\hbar}. \quad (4)$$

We can also express the effective Rabi frequency in terms of the total laser intensity I_{tot}, the ratio of intensity of Raman beams q (I_2/I_1), the optical transition linewidth Γ, and the saturation intensity I_{sat} as

$$|\Omega_{eff}| = \frac{\Gamma^2\sqrt{q}}{4I_{sat}(1+q)}.\frac{I_{tot}}{\Delta} \quad (5)$$

Assuming all atoms are in state $|g\rangle$ at the beginning of interaction, the probability of atoms in excited state is given by

$$P_e(t) = \frac{1}{2}\left(1 - cos\Omega_{eff}T\right). \quad (6)$$

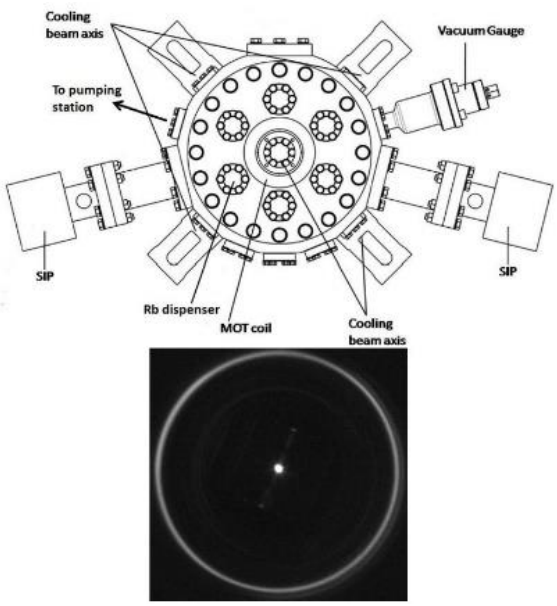

Figure 2: (a)Schematic of the Ti chamber. The cloud formation occurs at the centre. (b) Cold atom cloud captured in infrared camera via chamber viewport

The experimental setup includes compact vacuum subsystems, electronic rack consisting of laser controllers and drivers for modulators, an optical module for beam modulation and fiber coupling, and a data acquisition/processing module. Our vacuum system consists of a Titanium-made ultra-high vacuum chamber (2.2 L, 20 cm diameter), two sputter ion pumps (SIPs), a non-evaporable getter (NEG) pump, and vacuum gauge. The schematic of the UHV chamber is shown in Fig. 2 a. SIPs (SAES) are kept in the ON state to maintain the constant vacuum (10^{-10} mbar). The Rb dispenser (SAES 5G0125) is placed inside the chamber and activated by an electrical feed-through.

Cooling Rb Atoms

The viewports of UHV camber are constructed with in-house made adapters to attach beam collimators ensuring orthogonal orientation, enabling all six cooling beams to enter and access the trap center. The Magneto Optical Trap (MOT) coils are attached to the chamber with recessed flanges that align themselves with the horizontal cooling axis. A constant current of 3 A is driven in coils to generate the trapping quadrupole magnetic field ($\partial B/\partial z = 12G/cm$). Details of the cold atom cloud generation from Rb vapour is described in previous report [27]. The cooling laser beam is red detuned by 18 MHz from $5^2S_{1/2}\ F = 2 \rightarrow 5^2P_{3/2}\ F = 3$ [24] transition and repumping laser beam resonant to $5^2S_{1/2}\ F = 1 \rightarrow 5^2P_{3/2}\ F = 2$, are used for MOT formation. Fig. 2 b shows the photograph of a cloud with temperature 8.5 μK viewed using an IR camera (pco.pixelfly). Repumping beam is switched off ($3ms$) earlier than cooling beam to prepare cold atoms in F = 1 ground level.

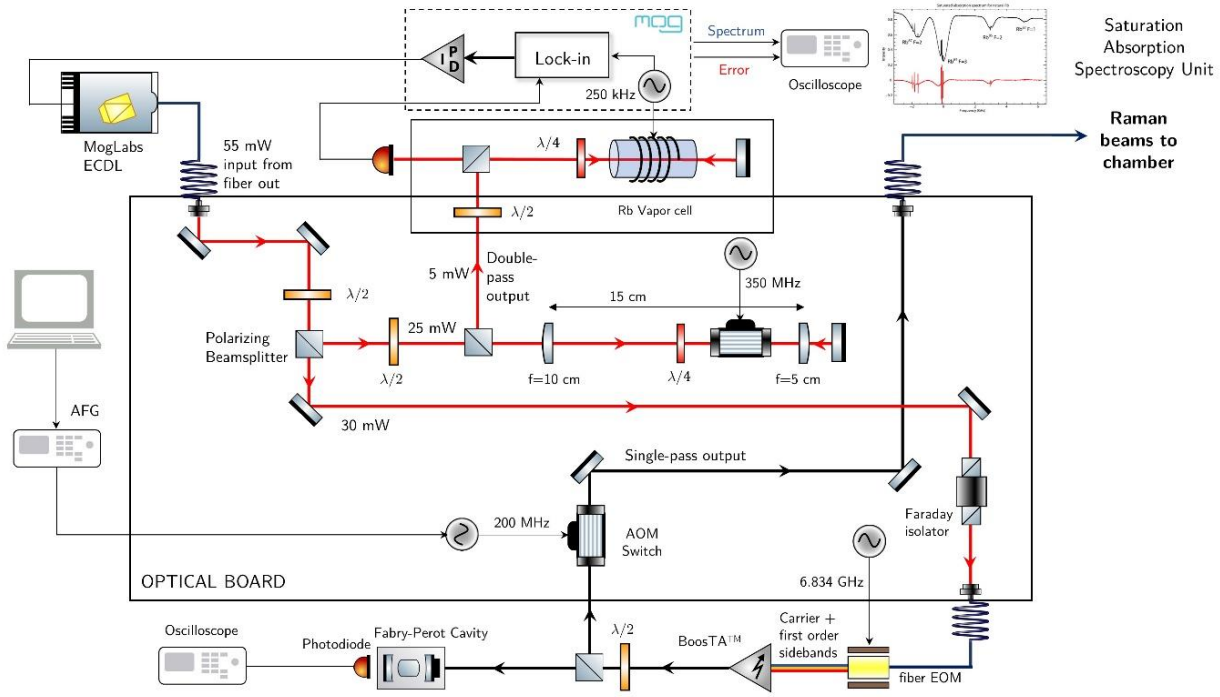

Figure 3: Schematic of Raman beam generation setup.

Raman Beam Generation for Rabi Oscillations

Experimental implementation of Raman beams primarily involves generation of two laser beams with frequency difference of ω_{HFS} $(\omega_1 - \omega_2)$, detuning the laser beam frequency by Δ from the excited state and switching the beam with a response time of few μs. A portion of the Raman seed laser beam generated from Moglabs ECDL is modulated using a free space AOM in double pass configuration. This beam (ω_1) generates the blue shifted saturation absorption spectrum. The laser is thus frequency locked to $5^2S_{1/2} \rightarrow 5^2P_{3/2}$ transition in order to supply an overall red detuning $\Delta = 1.8$ GHz from $5^2S_{1/2}\, F = 1 \rightarrow 5^2P_{3/2}\, F = 1$ transition. The second portion of laser beam is modulated using a fiber Electro Optic Modulator (EOM) modulated with a frequency close to ω_{HFS} that generates carrier and side bands $(\omega_1, \omega_1 \pm \omega_{HFS})$. By locking ω_1 detuned by Δ, the $\omega_1 - \omega_{HFS}$ side band becomes resonant to $F = 2 \rightarrow F' = 1$. The $\omega_1 + \omega_{HFS}$ side band will be far detuned away from all the 3 level transitions in the system. The EOM output beam is amplified using laser amplifier and the amplified beam is switched in μs using an Acousto Optic Modulator (AOM). Detailed schematic of the Raman beam setup is shown in Fig. 3. A Faraday isolator is placed before fiber-coupling in order to avoid back-reflection from the amplifier chip. A small portion of the amplified output beam is supplied to Fabry Perot Interferometer (FPI) to monitor the intensity ratio between side band and carrier. This was performed to ensure that the differential AC shift cancellation is holding during the measurement. Raman beams are switched at μs precision by passing through an AOM and later coupled into high power optical fiber. The beams are supplied into the UHV chamber using a collimator in $\sigma^+ - \sigma^+$ polarization and aligned with the MOT cloud in co-propagating configuration. Subsequent to cooling, the cold atom cloud is released from the trap and the pair of Raman beams of total power 60 mW is applied to the cloud vertically from the top.

Experimental Sequence

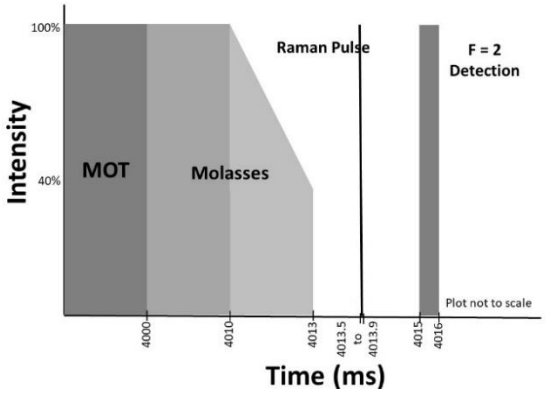

Figure 4: Experimental sequence to extract the Rabi oscillations. The Raman pulse width is changed from 0 to 400 µs with a step size of 10 µs

To study the response of atoms to applied Raman beams, the implemented experimental sequence is shown in Fig. 4. The cold atoms are made to interact with the Raman beams by switching ON the AOM after releasing from the trap. The duration of Raman pulses and the frequency are controlled externally and atom population in two ground states is detected after interaction with Raman beams using detection beams resonant to their transitions. After the interaction, the number of atoms present in ground state $F = 2$ is detected by fluorescence imaging technique. Detection beam resonant to the transition $F = 2 \rightarrow F' = 3$ applied and the atom population in state $F = 2$ is measured from the fluorescence. The oscillations experimentally extracted are shown in Fig.5. The Raman pulse duration is varied in steps of μs and the relative population of atoms in $F = 2$ energy level is measured.

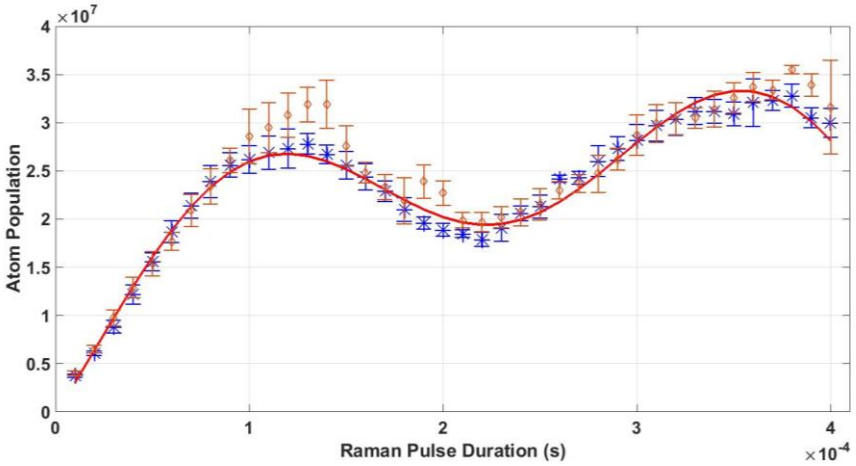

Figure 5: Atom population in F = 2 for different Raman pulse width. The blue and orange points are mean atom population observed for total Raman power = 60 mW, Δ = 1.8 GHz from two measurement sets and red trace is the sinusoidal fit (R2 = 0.979). The Raman induced population transfer is oscillating over a period of 220 μs, which is well matching with the theoretical value given by eq. (5).

A damped version of probability of finding atoms in this state after Raman pulse was fitted to data as shown in the red trace. The fitted Rabi frequency is 23 kHz. The high damping of

oscillation is due to the wide velocity distribution of initial cloud and incomplete population transfer due to lack of magnetic state selection step. A frequency of 29 kHz Rabi oscillation was obtained through theoretical calculation in agreement with the observed oscillation. The Raman beam intensity experienced by cold atoms are less than the intensity of beams measured. The oscillations are damped rapidly for longer pulse duration due to addressing the less number of atoms. This measurement of Rabi frequency is helpful in determining the pulse duration for the $\pi/2$ (beam splitter), π (mirror) pulses which becomes the sequence to coherently divide, deflect and finally recombine an atomic wave-packet in three pulse interferometers.

RAMSEY FRINGES

Ramsey fringes is an example of a basic atom interference. After applying a $\pi/2$ pulse, we allow the cloud to undergo a long free evolution. This followed by another $\pi/2$ pulse closes a basic interferometer and produces Ramsey fringes. This can be understood for the case of a two-level system by following the arguments given by Cohen-Tannoudji and Guery-Odelin [23]. Consider the following Hamiltonian.

$$H = \frac{\hbar\omega_o}{2}(|e\rangle\langle e| - |g\rangle\langle g|) + \frac{\hbar\Omega(t)}{2}\left(e^{i\omega_L t}|e\rangle\langle g| + e^{-i\omega_L t}|g\rangle\langle e|\right), \quad (7)$$

where $|g\rangle, |e\rangle$ are the two levels of the system with energy $-\hbar\omega/2$ and $+\hbar\omega/2$ respectively, ω_0 is the frequency separation between the levels, ω_L is the external laser frequency, and the Rabi frequency is given by Ω. The second part of the Hamiltonian is the interaction part which we will denote by H_I. We are assuming that the field amplitude is sufficiently small for the perturbative treatment of H_I and the time evolution operator $U(t_f, t_i)$ is limited only to the first order in $\Omega(t)$. The transition probability from one state to other is given by

$$\left|\langle g|U(t_f, t_i)|e\rangle\right|^2 = \left|\frac{1}{2}\, e^{-\frac{i\omega_o(t_f+t_i)}{2}} \times \int_{t_i}^{t_f} \Omega(t) e^{\frac{i(\omega_o-\omega_L)t}{2}}\, dt\right|^2. \quad (8)$$

Now, the time variable is changed to $t' = t - t_p$, where t_p is the peak time of the interaction pulse. Since the pulse width is much smaller than $t_f - t_p$ and $t_p - t_i$, we can extend the limit of the integral to $\pm\infty$ and eq. (8) becomes

$$\left|\langle g|U(t_f, t_i)|e\rangle\right|^2 = \left|\frac{1}{2}\, e^{-\frac{i\omega_o(t_f+t_i)}{2}}\, e^{i(\omega_o-\omega_L)t_p} \times G(\omega_0 - \omega_L)\right|^2. \quad (9)$$

Here $G(\omega_0 - \omega_L)$ is the Fourier transform of $\Omega(t + t_p)$. Now, consider our case where two coherent pulses of duration $\tau_{\pi/2}$ are applied at t_a and t_b respectively with $t_b - t_a = T \gg \tau_{\pi/2}$. The total amplitude is the sum of amplitudes associated with each pulse, and hence

$$\left|\langle g|U(t_f, t_i)|e\rangle\right|^2 = \frac{1}{4}|G(\omega_0 - \omega_L)|^2 \times \left|\left(e^{i(\omega_o-\omega_L)t_a} + e^{i(\omega_o-\omega_L)t_b}\right)\right|^2.$$

$$= \frac{1}{4}\left|G(\omega_0 - \omega_L)[1 + e^{i(\omega_o - \omega_L)T}]\right|^2 = \left|G(\omega_0 - \omega_L)\cos[\frac{(\omega_o - \omega_L)T}{2}]\right|^2 \quad (10)$$

It is clear that the transition probability exhibits interference fringes with a fringe spacing of $2\pi/T$. A scan of the frequency difference is realized by varying the EOM frequency. The population ratio is obtained by the same procedure discussed in [24]. Fig. 6 shows the Ramsey fringes obtained in a co-propagating configuration. The T used is 2 ms, and the fringe spacing is $\sim$ 3 kHz, which is well matching with the theoretical values. Ramsey fringes obtained in a co-propagating configuration can be identified as the first step towards a full interferometer sequence.

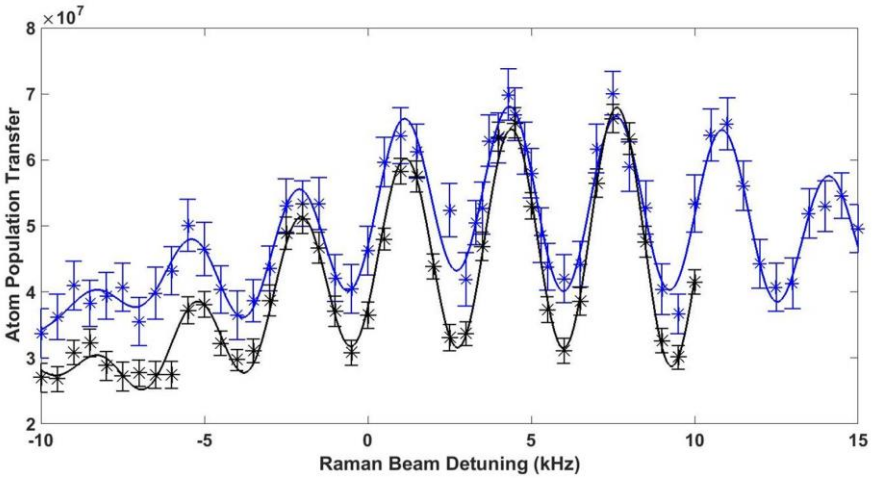

Figure 6: Ramsey fringes from two measurement sets with T = 2ms. Black and blue traces are guide for the eye.

CONCLUSION

In our study, we have accomplished the coherent manipulation of cold atoms by stimulated Raman transition. This step plays an important role in manipulating atomic ensemble to follow the parallelogram trajectory and undergo interference. We have successfully obtained sustained Rabi oscillation frequency and characterized the π and $\pi/2$ pulse duration. Subsequently, we have characterised the Ramsey fringes in co-propagating configuration with fixed Raman pulse width. This is the initial step towards realizing a cold atom interferometer for gravity measurements.

We have optimized the parameters such as the Raman beam intensity, the frequency separation, the intensity ratio of beams and the frequency lock of lasers. The $\pi/2$ pulse duration of 55 μs, determined from the obtained Rabi frequency is applied for characterizing Ramsey fringes. The co-propagating configuration of Raman beams made it convenient to obtain the transitions as they become Doppler insensitive. Presently, we are using compensation coils to eliminate effects of background magnetic field in the interaction region. But we plan to use mu-metal shield in our setup to eliminate such effects along with facilitating efficient cooling. We also intend to proceed towards counter propagating configuration to impart the momentum transfer between the atomic states, which is an important attribute of two photon transitions for atom interferometry.

Author Contributions

Hriday Dath and S. Kannan contributed to the paper equally and are the first authors. V. N. Radhika supervised the whole work. All the authors have contributed to the final version of the manuscript.

References

[1] G. Rosi, F. Sorrentino, L. Cacciapuoti, M. Prevedelli, and G. M. Tino, Nature, 510, 518-521 (2014)

[2] P. Asenbaum, C. Overstreet, M. Kim, J. Curti, and M. A. Kasevich, Physical Review Letters, 125, 191101 (2020)

[3] L. Morel, Z. Yao, P. Clade, and S. Guellati-Khelifa, Nature, 588, 61-65 (2020)

[4] J. Dalibard, and C. Cohen-Tannoudji, Journal of the Optical Society of America B, 6, 11 (1989)

[5] J. Grosse, S. T. Seidel, D. Becker, M. Lachmann, D. Maike, M. Scharringhausen, C. Braxmaier, and E. M. Maria, Journal of Vacuum Science &Technology A: Vacuum, Surfaces, and Films, 34, 031606 (2016)

[6] M. D. Lachmann, H. Ahlers, D. Becker, A. N. Dinkelaker, J. Grosse, O. Hellmig, H. Muntinga, V. Schkolnik, S. Seidel, and T. Wendrich, Nature communications, 12, 1‑6 (2021)

[7] M. Wright, L. Anasrassiou, C. Mishra, J. Davies, A. Phillips, S. Maskell, and J. Ralph, Frontiers in Physics, 927 (2022)

[8] R. Geiger, A. Landragin, S. Merlet, and F. Pereira Dos Santos, AVS Quantum Science, 2, 024702 (2020)

[9] A. Bertoldi et al., Experimental Astronomy, 51, 1417‑1426 (2021)

[10] K. Bongs et al., Nature Reviews Physics, 1, 731-739 (2019)

[11] X. Wu et al., Science advances, 5, 20 (2019)

[12] V. Menoret et al., Scientific reports, 8, 1-11 (2018)

[13] B. Stray et al., Nature, 602, 590-594 (2022)

[14] Y. Bidel et al., Nature communications, 9, 1-9 (2018)

[15] S. M. Brewer et al., Physical review letters, 123, 033201 (2019)

[16] K. Varga-Umbrich et al., The European Physical Journal D, 76, 1-11 (2022)

[17] Y. Wang et al., Physical Review Research, 4, L022058 (2022)

[18] S. Rosi et al., Scientific reports, 8, 1-9 (2018)

[19] R. C. Das, D. Shylla, A. Bera, and K. Pandey, Journal of Physics B: Atomic, Molecular and Optical Physics 56, 2, 025301 (2023)

[20] Ch. J. Borde, Physics letters A, 140, 10-12 (1989)

[21] M. Kasevich and S. Chu, Physical review letters, 67, 181 (1991)

[22] M. Kasevich and S. Chu, Foundations of Quantum Mechanics, 47-54 (1992)

[23] C. Cohen-Tannoudji and D. Guery-Odelin, Advances in atomic physics: an overview, World scientific (2011)

[24] D. A. Steck, Rubidium 87 D line data, (2001)

[25] Devani D et al. CEAS Space J., 12, 539-549 (2020)

[26] Lyu W et al. Phys. Rev. Appl., 18, 054091 (2022)

[27] Dath H et al. Res Rev J Pure Appl Phys., (2023)

[28] Janvier, C et al. Phys. Rev. A, 105, 022801 (2022)

[29] Burrow, S et al. Optics Express, 19, 044015 (2023)

[30] Dyer, S et al. Physical Review Applied, 31, 40871‑40880 (2023)